Published in final edited form as:
J Magn Reson Imaging. 2010 March ; 31(3): 645–654. doi:10.1002/jmri.22058.

Carotid Arterial Wall MRI at 3T Using 3D Variable-Flip-Angle TSE with Flow-Sensitive Dephasing

Zhaoyang Fan, MS[1,2], **Zhuoli Zhang, MD, PhD**[1], **Yiu-Cho Chung, PhD**[3], **Peter Weale, BA, DCR (R)**[3], **Sven Zuehlsdorff, PhD**[3], **James Carr, MD**[1], and **Debiao Li, PhD**[1,2]

[1] Department of Radiology, Northwestern University, Chicago, Illinois

[2] Department of Biomedical Engineering, Northwestern University, Evanston, Illinois

[3] Siemens Medical Solutions USA, Inc., Chicago, Illinois

Abstract

Purpose—To evaluate the effectiveness of flow-sensitive dephasing (FSD) magnetization preparation in improving blood signal suppression of three-dimensional (3D) turbo spin-echo (TSE) sequence (SPACE) for isotropic high-spatial-resolution carotid arterial wall imaging at 3T.

Materials and Methods—The FSD-prepared SPACE sequence (FSD-SPACE) was implemented by adding two identical FSD gradient pulses right before and after the first refocusing 180°-pulse of the SPACE sequence in all three orthogonal directions. Nine healthy volunteers were imaged at 3T with SPACE, FSD-SPACE, and multislice T2-weighted two-dimensional (2D) TSE coupled with saturation band (SB-TSE). Apparent carotid wall-lumen contrast-to-noise ratio ($aCNR_{w\text{-}l}$) and apparent lumen area (aLA) at the locations with residual-blood signal shown on SPACE images were compared between SPACE and FSD-SPACE. Carotid $aCNR_{w\text{-}l}$ and lumen (LA) and wall area (WA) measured from FSD-SPACE were compared to those measured from SB-TSE.

Results—Plaque-mimicking flow artifacts identified in 7 carotids on SPACE images were eliminated on FSD-SPACE images. The FSD preparation resulted in slightly reduced $aCNR_{w\text{-}l}$ ($p = 0.025$), but significantly improved aCNR between the wall and residual-blood regions ($p < 0.001$) and larger aLA ($p < 0.001$). Compared to SB-TSE, FSD-SPACE offered comparable $aCNR_{w\text{-}l}$ with much higher spatial resolution, shorter imaging time, and larger artery coverage. The LA and WA measurements from the two techniques were in good agreement based on intraclasss correlation coefficient (0.988 and 0.949, respectively; $p < 0.001$) and Bland-Altman analyses.

Conclusion—FSD-SPACE is a time-efficient 3D imaging technique for carotid arterial wall with superior spatial resolution and blood signal suppression.

Keywords

carotid artery; magnetic resonance imaging; atherosclerosis; 3D SPACE; black-blood

Introduction

Carotid atherosclerosis is a degenerative disease of the arterial wall which can result in predisposition to cerebral thrombo-embolic stroke, the leading cause of mortality and morbidity worldwide (1). Previous studies suggested that high-risk atherosclerotic plaques can be identified in terms of plaque composition and morphology (2,3).

Corresponding Author (Reprint Info): Debiao Li, Ph.D., Department of Radiology, Northwestern University, 737 N. Michigan Ave, Suite 1600, Chicago, IL 60611, Phone: (312) 926-4245, FAX: (312) 896-5665, d-li2@northwestern.edu.

High-spatial-resolution MRI with blood signal suppression (i.e., black-blood, BB) has emerged as the leading noninvasive imaging modality allowing for directly visualizing diseased vessel wall, characterizing plaque components, and thus assessing plaque vulnerability in vivo (4-6).

BB MRI is typically performed using a single-slice two dimensional (2D) turbo spin-echo (TSE) sequence, in conjunction with a double inversion-recovery (DIR) preparation (7,8) or a spatial presaturation band (SB) (9). TSE offers flexible tissue contrast, less sensitivity to magnetic field inhomogeneities, and high signal-to-noise ratio (SNR) (10,11). 2D TSE, however, is restricted to cross-sectional imaging in order to maximize inflow or outflow of the pre-labeled blood spins, thereby compromising scan time-efficiency. While several BB multislice TSE techniques have been developed to speed up acquisition (12-15), their blood-suppressing performance may be degraded by complex flow patterns (slow, stagnant, or recirculating flows) at the carotid bifurcation or by the large slice number (16). Additionally, a common problem in 2D imaging is the poor spatial resolution in the slice-select direction, making images more prone to the partial volume effect and thus obscurity of fine plaque structures. In contrast, three-dimensional (3D) imaging has several advantages: (a) intrinsic high SNR that may be traded for high spatial resolution; (b) improved anatomic coverage via a longitudinal acquisition; (c) capability of retrospective visualization of vessel wall from arbitrary angle using multiplanar reconstruction (MPR).

For 3D vessel wall imaging, two challenges need to be addressed: acquisition time and blood flow suppression. Long imaging times and suboptimal BB appearance will make 3D images more susceptible to motion artifacts and plaque-mimicking flow artifacts, respectively. Previous investigators have applied 3D TSE (17) and gradient and spin-echo (GRASE) (18) sequences combined with field-of-view (FOV) reduction techniques and DIR preparation for BB MRI that again limits the 3D slab's thickness and positioning (19). A flow-sensitive dephasing (FSD) magnetization preparation scheme can be another approach to blood signal suppression (20-22). 3D balanced steady-state free precession (bSSFP) coupled with this scheme has proved to be a fast carotid arterial wall imaging method at 1.5T (21). At 3T, however, bSSFP suffers from off-resonance artifacts that may degrade vessel wall conspicuity (23); recently, 3D TSE with variable-flip-angle refocusing RF pulses (SPACE) was introduced as a candidate due to its insensitivity to magnetic field inhomogeneities (24). Despite its inherent flow-void capability, SPACE images may still exhibit plaque-mimicking artifacts due to insufficient blood suppression at the carotid bifurcation. Thus, further improvement in blood signal suppression with SPACE is desired.

In this work, we incorporated a modified FSD preparation scheme into the SPACE sequence to improve its BB effect. The radio-frequency (RF) pulse series ($90°_{x}$-$180°_{y}$-$90°_{-x}$) in the conventional FSD preparation was not used; instead, FSD gradient pulses were symmetrically placed around the first refocusing 180° pulse of the SPACE sequence to impart flow sensitization. The FSD-prepared SPACE (FSD-SPACE) sequence was compared with SPACE with respect to blood signal suppression. In addition, the feasibility of FSD-SPACE for carotid arterial wall imaging with submillimeter isotropic spatial resolution was investigated, using multislice T2-weighted 2D TSE coupled with SB (SB-TSE) as a reference that is a commonly used BB MRI technique (25,26).

Materials and Methods

Theory and Modification of SPACE Imaging Sequence

Compared with conventional 3D TSE where high-flip-angle RF pulses are used, SPACE employs variable low-flip-angle nonselective refocusing RF pulses to achieve near constant echo amplitudes over long echo trains, which is advantageous for reducing acquisition time

and RF power deposition (Fig. 1a) (27,28). The SPACE sequence has an in-plane BB property primarily due to motion-induced intravoxel dephasing among the blood spins (29,30). This kind of phase dispersion arises from the intravoxel blood flow velocity variation as well as the uncompensated first-order gradient moment (ignoring higher-order gradient moments without loss of generality) during each echo readout. Blood signal can be effectively attenuated as the dephasing reaches an adequate level. In particular, this phenomenon becomes more apparent if the blood flow is parallel to the readout direction in that the first-order gradient moment generated in this direction is substantially higher than in other two directions. Additionally, the low-flip-angle refocusing pulses also introduce stimulated echoes which may have different first-order gradient moments compared with the corresponding spin-echoes, leading to further phase dispersion. On the other hand, unlike the case of using ideal 180° refocusing pulses where the dephasing can be canceled for every even echo, the dephasing will accumulate over the long echo train.

The previously used FSD preparation module for blood signal suppression consists of a $90°_{x}$-$180°_{y}$-$90°_{-x}$ nonselective RF pulse series and symmetric FSD gradient pulses around the center $180°_{y}$ RF pulse in the readout, phase encoding, and slice directions, respectively (20-22). The underlying blood suppression mechanism also relies on intravoxel phase dispersion that develops among the flowing blood spins, as opposed to the stationary spins, during the application of the FSD gradient pairs. The FSD gradient-$180°_{y}$ -FSD gradient sequence structure is essential for imparting the flow sensitization to the blood spins that have been flipped to the transversal plane.

To further improve the BB effect of SPACE, the above FSD mechanism is exploited in this work. Specifically, the FSD-SPACE sequence was implemented on a clinical 3T scanner by adding two identical flow-sensitizing trapezoidal gradient pulses right before and after the first refocusing 180°-pulse in all three orthogonal directions, as shown in Fig. 1b. The duration and amplitude of each pair of FSD gradients were set to 3 msec and 12 mT/m, respectively, resulting in an accumulative first-order gradient moment (m_1) of 256 $mT{\cdot}ms^2/m$ and a b-value of 0.86 s/mm^2. These values were determined empirically to achieve low signal intensity (SI) in the carotid lumen while maintaining adequate SI in surrounding tissues.

Study Population

Nine healthy volunteers (8 males, 1 female; age range 28-72 years with mean 47 years) were recruited in the study approved by the university's institutional review board. Written informed consent was obtained from all participants. To minimize motion artifacts, subjects were instructed to breathe normally and abstain from swallowing during scans.

Imaging System

Imaging was performed on a 3T whole-body MR system (MAGNETOM Trio; Siemens AG Healthcare, Erlangen, Germany). The scanner's integrated body coil was used for RF signal transmission. A bilateral four-channel phased array carotid surface coil (Machnet, Eelde, The Netherlands) was used for signal reception.

Imaging Protocol

The bilateral carotid artery bifurcations were initially localized using a tri-plane turbo fast low angle shot (FLASH) sequence followed by a multislice 2D time-of-flight (TOF) transverse acquisition. The following three vessel wall scans covering bilateral carotid artery bifurcations as well as the proximal portions were performed subsequently.

Conventional SPACE—An oblique coronal 3D imaging slab centered at the carotid bifurcations was prescribed based on the TOF angiogram (Fig. 2). Imaging parameters

included: repetition time (TR)/echo time (TE) = 1600/175 ms, turbo factor = 70, FOV = 160×116×50 mm^3, matrix size = 256×186×80 (yielding an 0.63-mm isotropic spatial resolution), signal average = 2, parallel imaging (GRAPPA acceleration factor = 2) along the phase-encoding direction, receiver bandwidth = 454 Hz/pixel (echo spacing = 4.5 ms), acquisition time = 6.4 min. The variable-flip-angle scheme used in both SPACE and FSD-SPACE acquisitions is illustrated in Fig. 3. To maximize the flow-void effect, readout (i.e. frequency encoding) was set in the superior-inferior direction, approximately parallel to the carotid's long axis. Linear k-space ordering was used in the phase-encoding and partition-encoding directions.

Spectrally-selective fat saturation RF pulse preceded data acquisition to suppress signal from perivascular fat. Electrocardiographic (ECG) triggering was not used.

FSD-SPACE—The identical imaging slab as used above was prescribed. The imaging parameters, except for TE which was increased to 181 ms due to the addition of the FSD gradient pulses, remained unchanged. Acquisition time = 6.4 min. The same FSD sensitization (gradient duration = 3 msec, gradient amplitude = 12 mT/m) was applied in the readout, phase-encoding, and partition-encoding directions, respectively, as suggested in the previous literature (21).

Multislice 2D SB-TSE—A multislice T2-weighted 2D SB-TSE sequence was employed to provide reference images. ECG triggering was not used according to literature (25). A total of 16 transverse slices centered at the carotid bifurcations were collected through two interleaved scans, achieving no inter-slice gap and taking 1.6 min per scan (Fig. 2). Two 50-mm-thick saturation bands, 10 mm above and below the imaging stack, were used to suppress blood signal. Imaging parameters were as follows: TR/TE = 2500/54 ms, turbo factor = 13, FOV = 140×140 mm^2, matrix size = 256×256 (yielding 0.55×0.55 mm^2 in-plane spatial resolution), slice thickness = 3 mm, inter-slice gap = 3 mm, signal average = 2, spectrally-selective fat saturation, receiver bandwidth = 490 Hz/pixel (echo spacing = 7.7 ms), flip angle = 180°.

Image Analysis

Analysis was focused on the carotid bifurcation since this site is often afflicted with complex flow patterns and thus flow artifacts in dark-blood MRI.

Comparison between SPACE and FSD-SPACE—3D datasets from the conventional SPACE scan were reviewed by an experienced radiologist using MPR on a workstation (Leonardo; Siemens AG Healthcare, Erlangen, Germany) to identify the possible residual flow artifacts at either left or right carotid bifurcation. From each carotid artery with flow artifacts, five 2D cross-sectional 0.63-mm-thick slices within the artifactual region were reconstructed from the 3D SPACE and FSD-SPACE image sets, respectively, with the slice location exactly matched. The data of subjects with no flow artifacts identified on conventional SPACE images was excluded from this comparison analysis.

Signal measurements were performed on those reconstructed 2D images using free image processing software, ImageJ (National Institutes of Health, Bethesda, MD, USA). Lumen signal (S_l) was measured as the mean SI within an ROI manually drawn to cover the entire arterial lumen. Arterial wall signal (S_w) was measured as the mean SI of a one-pixel-width circumferential path traced manually through the middle of the arterial wall (31). This approach is expected to mitigate SI measurement inaccuracy potentially due to the partial volume effects when near-boundary residual blood signal or nonideal perivascular fat saturation is present. Here, the lumen ROI and path were prescribed on FSD-SPACE images and then propagated to the corresponding conventional SPACE images, assuming that the former scan can yield

relatively cleaner arterial lumen. Noise level (σ_n) was measured as the standard deviation of signal from an ROI manually drawn in the adjacent homogenous sternocleidomastoid muscle because of inhomogeneous noise distribution on images acquired using parallel imaging (32, 33). Care was taken to ensure that the noise ROIs were matched in size (> 20 mm^2) and location between the two 3D scans. We thereby referred to the calculated SNR for the carotid lumen and wall as apparent SNR ($aSNR_l$, $aSNR_w$) that was calculated by $aSNR = S/\sigma_n$, where S denotes S_l or S_w. Apparent wall-lumen contrast-to-noise ratio ($aCNR_{w-l}$) for each location were calculated as

$$aCNR_{w-l}=aSNR_w - aSNR_l \quad [1]$$

In addition to the above apparent CNR of entire lumen, the apparent CNR between the residual-blood (rb) region, which appeared to connect with vessel wall (Fig. 4), and the surrounding vessel wall ($aCNR_{w-rb}$) was also measured because this value implies the likelihood of mistaking this region for part of the thickening wall or atherosclerotic lesion. Unlike lumen-ROI-prescription method described above, a residual-blood ROI was delineated on conventional SPACE images, with the matched FSD-SPACE images as reference to indicate the inner wall boundary, and then propagated to the matched FSD-SPACE images, as shown in Fig. 4.

Finally, as a further measure of the BB effect of the FSD preparation, the apparent lumen area (aLA) was independently measured using ImageJ on both FSD-SPACE and SPACE 2D images by an experienced author blinded to the techniques used. For this purpose, the residual flow signal was considered part of vessel wall only when it could not be visually isolated from the inner wall boundary.

Comparison between FSD-SPACE and 2D SB-TSE—At the carotid bifurcation, 5 locations per artery were chosen from the 2D SB-TSE image sets and 5 location-matched (based on spatial information on 2D TSE images) transverse 2D images were then reconstructed from the 3D FSD-SPACE datasets using MPR. The thickness of the reconstructed images was specified based on different purposes. For $aCNR_{w-l}$ comparison, the created 2D images were 0.63 mm in thickness, retaining an isotropic voxel size, whereas for morphology comparison, we made 3-mm-thick slices in order to test whether the two acquisitions would provide consistent measurements of carotid wall (WA) and lumen areas (LA) in the absence of difference in slice thickness.

Signal measurements were performed on each 2D image pair obtained with FSD-SPACE and SB-TSE in the same manner as described in previous section except that the one-pixel-width paths in the arterial wall and the ROI in the lumen were drawn independently on each image. To take into account the variation in voxel size, the measured carotid $aCNR_{w-l}$ was further normalized by the voxel volume (in units of cubic millimeters), giving rise to a CNR per unit voxel ($aCNR_{uv}$).

To measure arterial wall and lumen areas, the inner and outer wall boundaries were manually outlined, leading to two ROIs, independently on the matched 2D image sets from the FSD-SPACE and SB-TSE scans. The inner ROI was used for lumen area measurement and the wall area was calculated as the difference in areas between the two ROIs.

Statistical Analysis

SPSS (SPSS Inc., Chicago, IL, USA) was used to perform the statistical analysis. All quantitative measurements including $aSNR_l$, $aSNR_w$, $aCNR_{w-l}$, $aCNR_{w-rb}$, and aLA were

compared between the FSD-SPACE and conventional SPACE techniques using a two-tailed paired Student's *t*-test. The same test was also conducted on $aCNR_{w\text{-}l}$, CNR_{uv}, LA, and WA to compare the FSD-SPACE versus SB-TSE techniques. Furthermore, agreement in WA and LA measurements obtained from the two techniques was assessed through intraclass correlation coefficient (ICC) (34) and Bland-Altman plots (35). In all tests, statistical significance was defined at the $p < 0.05$ level. Data were presented as means ± standard deviations.

Results

Comparison between SPACE and FSD-SPACE

The FSD-SPACE and conventional SPACE image sets were successfully obtained from all 9 volunteers. The residual blood signal was visually identified around the carotid bifurcations in 5 volunteers (2 with both carotids and 3 with one carotid) on conventional SPACE images, which were dramatically suppressed on FSD-SPACE images. Representative images illustrating this improvement are shown in Fig. 4 and Fig. 5. Some of the intraluminal signal is connected with the surrounding vessel wall and thus could potentially be mistaken for a plaque, whereas others is isolated from vessel wall. Associated with blood signal suppression by the FSD preparation, overall signal attenuation was appreciable. However, the vessel wall boundaries were still discernable at the chosen FSD gradient parameters.

Quantitative measurements and statistical analyses are summarized in Table 1. In the 35 locations (7 carotids) analyzed, FSD resulted in a significantly decreased $aSNR_l$ (6.5 ± 2.4 on SPACE vs. 3.6 ± 1.1 on FSD-SPACE, $p < 0.001$) but inevitably a sacrificed $aSNR_w$ (14.2 ± 3.6 on SPACE vs. 10.7 ± 2.2 on FSD-SPACE, $p < 0.001$). The consequence is that $aCNR_{w\text{-}l}$ was slightly reduced (7.7 ± 1.8 on SPACE vs. 7.1 ± 1.4 on FSD-SPACE, $p = 0.025$). However, in the residual-blood region rather than the entire lumen, $aCNR_{w\text{-}rb}$ was significantly improved with FSD-SPACE (0.8 ± 2.3 on SPACE vs. 4.7 ± 2.2 on FSD-SPACE, $p < 0.001$). Moreover, a significantly increased aLA was also obtained with FSD-SPACE, as illustrated in Table 1 and Fig. 4.

Comparison between FSD-SPACE and 2D SB-TSE

Seven out of 9 volunteers underwent both 3D FSD-SPACE and multislice 2D SB-TSE scans with acceptable image quality. Representative images obtained with the two techniques in a volunteer are shown in Fig. 6. At the carotid bifurcations, delineation of the carotid arterial wall and suppression of intraluminal blood signal were generally comparable between the two image sets. However, the residual blood signal was present in a few slices on SB-TSE images, indicating suboptimal blood signal suppression associated with the SB technique and multislice acquisition. The 3D acquisition using FSD-SPACE enabled visualization of the arterial wall from arbitrary orientations, particularly from the long-axis and truely orthogonal views, which is impossible with the 2D acquisition (Fig. 7).

Quantitative measurements and statistical analyses were listed in Table 2. A total of 70 transverse locations from 14 carotids were used for quantitative analyses. There was no difference in $aCNR_{w\text{-}l}$ between the 3D and 2D acquisitions (6.8 ± 2.1 on SB-TSE vs. 7.0 ± 2.1 on FSD-SPACE, $p = 0.329$). However, the 3D protocol offered a significantly improved $aCNR_{uv}$.

Morphological measurements of carotid LA and WA obtained from FSD-SPACE and SB-TSE were in a good agreement based on the ICC analysis (LA: ICC = 0.988; WA: ICC = 0.949; $p < 0.001$ for both) and the Bland-Altman plots (Fig. 8). However, there were, on average, a minor positive bias (2.7 ± 6.3% of average measurement) in LA measurements and a minor

negative bias (-5.6 ± 8.8% of average measurement) in WA measurements, respectively, with FSD-SPACE relative to SB-TSE. According to the paired t-test, those biases were statistically significant ($p < 0.001$).

Discussion

This study showed the effectiveness of the FSD magnetization preparation in improving SPACE's blood signal suppression. 3D isotropic high-spatial-resolution carotid arterial wall imaging using FSD-SPACE was achieved with comparable wall-lumen CNR and good agreement in wall and lumen area measurements with multislice T2-weighted 2D SB-TSE.

The carotid bifurcation is a site often afflicted with atherosclerosis. However, blood signal suppression is usually challenging in this location owning to the irregular geometry and complex flow patterns. Consequently, measurements of the vessel wall and plaque size are often inaccurate. In this work, the plaque-mimicking flow artifacts were observed in over half of the volunteers when using the conventional SPACE sequence. Substantial improvement in blood signal suppression was observed in the artifactual regions when incorporating SPACE with FSD preparation. Compared to conventional SPACE imaging, significantly elevated signal contrast (by approximately 6-fold) between those regions and the surrounding vessel wall sufficed to distinguish the lumen from inner wall boundary, effectively minimizing the likelihood of mistaking the flow artifacts for thickening wall.

We observed the overall signal loss when using the FSD preparation, which was also reported by previous studies (21,22). The CNR between the entire lumen and arterial wall was reduced by 8% in those cross-sections having flow artifacts. This reduction was contributed to the signal drop of 25% in the arterial wall, which presumably arose from T2 decay and diffusion attenuation associated with the FSD preparation. Several measures were made in this work to alleviate this side-effect. First, the three RF pulses ($90°_{x}$-$180°_{y}$-$90°_{-x}$) involved in the conventional FSD preparation were not used. Thus, the effective duration (i.e. T2-decay duration) of the FSD preparation was drastically shortened (7 ms), and, concomitantly, signal loss caused by otherwise added local B_1 and B_0 inhomogeneity was avoided. Second, the first-order gradient moment and *b*-value applied in our protocol were substantially lower than those employed in previous studies (21,22). This is because the SPACE sequence has an inherent BB effect and the FSD preparation simply acts as a supplement to SPACE acquisition for suppressing blood signal.

In this work, 3D FSD-SPACE was compared to multislice 2D SB-TSE with respect to wall-lumen CNR. Previous studies have shown that multislice 2D BB TSE imaging offers a higher tissue SNR efficiency (SNR normalized by imaging time pre section) and comparable wall-lumen CNR relative to single-slice 2D DIR-prepared TSE imaging (15). Although the DIR preparative sequence is more effective in suppressing blood signal compared to the SB method in the case of single-slice 2D imaging, these two techniques yield no significant difference in lumen SNR and wall-lumen CNR when multislice 2D acquisition is performed (25). Thus, multislice 2D SB-TSE was used in this comparison study.

The advantage of intrinsically high SNR/CNR with a 3D acquisition was demonstrated in this work. FSD-SPACE is capable of generating a comparable $aCNR_{w\text{-}l}$ while achieving a more than four-fold improvement in slice resolution over 2D SB-TSE. This high-spatial-resolution combined with adequate wall-lumen contrast renders this 3D imaging technique appropriate for plaque imaging in that the dimensions of individual plaque components are typically on the order of submillimeter (4). In an effort to avoid the partial volume effect, we employed the 3D FSD-SPACE sequence with an isotropic high resolution of $0.63\times0.63\times0.63$ mm^3. This protocol may facilitate plaque assessment with two major benefits. First, the fine plaque

structures can be better delineated, and extent and degree of plaques as well as the size of small plaque components can be reliably quantified. Second, misregistration of images obtained in serial examinations can be reduced because of flexible matching between 3D data sets, thereby allowing for accurate monitoring of disease progression and regression (19).

Good agreement of arterial wall and lumen area measurements between the 2D and 3D techniques was observed in this study. However, the LA values from FSD-SPACE were, on average, larger than those from SB-TSE; the WA values had an opposite finding. These biases are more likely to be explained by the fact that near-boundary blood signal was present in some transverse sections on 2D TSE images due to inadequate flow suppression by SB, as opposed to in-flow independent flow suppression in FSD-SPACE. It is anticipated that this discrepancy in morphological measurements would decline when comparing FSD-SPACE to single-slice 2D DIR-prepared TSE in which case the lumen can be sufficiently clean (19). While morphological evaluation was limited to cross-sections in this work, 3D imaging enables flexible viewing of the vessel wall that is desired for accurate quantitative measurement of disease burden in irregularly geometric plaques. (19) In contrast, it is impossible to acquire true cross-sectional views for all contiguous slices of both carotids within a single scan using a 2D imaging technique.

Large vessel coverage within a clinically practical scan time is another noteworthy advantage with FSD-SPACE imaging over its 2D counterpart. Oblique coronal acquisition and the associated improved BB effect make it possible to image carotids in a longitudinal manner, which is considerably time efficient. With the present SPACE protocol, a 12-cm-long carotid segment can be captured in around 6 min, whereas multislice 2D SB-TSE would take 8 min with slice resolution heavily sacrificed. Thus, this 3D sequence has the promise to serve as a plaque screening imaging approach.

The SPACE sequence used herein is of T2-weighting, but may involve certain T1 contrast due to the longitudinal magnetization recovery over the long echo train. For the purpose of assessing plaque composition, the SPACE sequence may need to be configured into different versions capable of T1-, T2-, and proton-density weighting contrasts (10). T1-weighted SPACE has been commercially available and investigated for carotid arterial disease imaging (36,37). To our knowledge, however, no study has been performed to systematically investigate multi-contrast SPACE imaging of atherosclerotic plaque.

Our study has a notable limitation related to motion that may be present in vessel wall caused by patient body movement, breathing, cardiac systolic pulsation, and swallowing. Compared to 2D imaging, 3D imaging is more sensitive to motion because imaging time is long and motion during a scan can affect the entire dataset. On the other hand, the application of the FSD preparation may exacerbate SPACE's susceptibility to motion owing to the motion-induced dephasing effect, resulting in reduced SNR in the regions with motion. Unfortunately, no compensation for vessel wall motion was performed during 3D scans in this study. We did notice more blurring artifacts or image quality degradation in 3D image sets in comparison to 2D image sets, a finding also reported previously (19). Although ECG triggering may not be necessary in 2D imaging (25), a recent work suggested a beneficial effect of ECG in submillimeter high-spatial-resolution 3D MRI of carotid vessel wall (38). Images acquired during diastole have shown less vessel blurring. In the case of SPACE imaging, ECG-triggering at every two cardiac cycles would not increase total imaging time compared to the present imaging protocol. However, blood flow is relatively slow during diastole, and stronger first-order gradient moment would be necessary to avoid otherwise more pronounced residual flow artifacts. Other motion-compensation methods, such as navigator-echo (39) or self-gating (40), have appeared to be able to reduce swallowing- and bulk motion-induced image artifacts and should readily be compatible with SPACE.

In addition, all subjects imaged in this study were healthy volunteers. Blood flow dynamics and subject tolerance to long scans may be quite different for patient group. Considering the complex flow patterns at or distal to a carotid atherosclerotic lesion, it is anticipated that an individually-tailored FSD configuration would be useful. As our ongoing work, for example, a quick scouting scan for appropriate first-order gradient moment may help yield good BB image quality. Nevertheless, the clinical value of FSD-SPACE needs to be investigated through a carotid atherosclerosis patient study.

In conclusion, this work demonstrated the effectiveness of the FSD magnetization preparation in improving blood signal suppression of SPACE for isotropic high-spatial-resolution 3D carotid arterial wall imaging at 3T. The superior spatial resolution and blood flow suppression along with high time-efficiency render this technique promising for vessel wall morphometry, plaque localization, and potentially characterization.

References

1. Ingall T. Stroke--incidence, mortality, morbidity and risk. J Insur Med 2004;36:143–152. [PubMed: 15301227]
2. Fuster V, Stein B, Ambrose JA, Badimon L, Badimon JJ, Chesebro JH. Atherosclerotic plaque rupture and thrombosis. Evolving concepts. Circulation 1990;82:II47–59. [PubMed: 2203564]
3. Falk E. Stable versus unstable atherosclerosis: clinical aspects. Am Heart J 1999;138:S421–425. [PubMed: 10539840]
4. Yuan C, Mitsumori LM, Beach KW, Maravilla KR. Carotid atherosclerotic plaque: noninvasive MR characterization and identification of vulnerable lesions. Radiology 2001;221:285–299. [PubMed: 11687667]
5. Fayad ZA. The assessment of the vulnerable atherosclerotic plaque using MR imaging: a brief review. Int J Cardiovasc Imaging 2001;17:165–177. [PubMed: 11587450]
6. Saam T, Hatsukami TS, Takaya N, et al. The vulnerable, or high-risk, atherosclerotic plaque: noninvasive MR imaging for characterization and assessment. Radiology 2007;244:64–77. [PubMed: 17581895]
7. Edelman RR, Chien D, Kim D. Fast selective black blood MR imaging. Radiology 1991;181:655–660. [PubMed: 1947077]
8. Simonetti OP, Finn JP, White RD, Laub G, Henry DA. “Black blood” T2-weighted inversion-recovery MR imaging of the heart. Radiology 1996;199:49–57. [PubMed: 8633172]
9. Felmlee JP, Ehman RL. Spatial presaturation: a method for suppressing flow artifacts and improving depiction of vascular anatomy in MR imaging. Radiology 1987;164:559–564. [PubMed: 3602402]
10. Yuan C, Mitsumori LM, Ferguson MS, et al. In vivo accuracy of multispectral magnetic resonance imaging for identifying lipid-rich necrotic cores and intraplaque hemorrhage in advanced human carotid plaques. Circulation 2001;104:2051–2056. [PubMed: 11673345]
11. Cai JM, Hatsukami TS, Ferguson MS, Small R, Polissar NL, Yuan C. Classification of human carotid atherosclerotic lesions with in vivo multicontrast magnetic resonance imaging. Circulation 2002;106:1368–1373. [PubMed: 12221054]
12. Song HK, Wright AC, Wolf RL, Wehrli FW. Multislice double inversion pulse sequence for efficient black-blood MRI. Magn Reson Med 2002;47:616–620. [PubMed: 11870851]
13. Parker DL, Goodrich KC, Masiker M, Tsuruda JS, Katzman GL. Improved efficiency in double-inversion fast spin-echo imaging. Magn Reson Med 2002;47:1017–1021. [PubMed: 11979583]
14. Yarnykh VL, Yuan C. Multislice double inversion-recovery black-blood imaging with simultaneous slice reinversion. J Magn Reson Imaging 2003;17:478–483. [PubMed: 12655588]
15. Mani V, Itskovich VV, Szimtenings M, et al. Rapid extended coverage simultaneous multisection black-blood vessel wall MR imaging. Radiology 2004;232:281–288. [PubMed: 15220509]
16. Steinman DA, Rutt BK. On the nature and reduction of plaque-mimicking flow artifacts in black blood MRI of the carotid bifurcation. Magn Reson Med 1998;39:635–641. [PubMed: 9543426]

17. Crowe LA, Gatehouse P, Yang GZ, et al. Volume-selective 3D turbo spin echo imaging for vascular wall imaging and distensibility measurement. J Magn Reson Imaging 2003;17:572–580. [PubMed: 12720267]
18. Luk-Pat GT, Gold GE, Olcott EW, Hu BS, Nishimura DG. High-resolution three-dimensional in vivo imaging of atherosclerotic plaque. Magn Reson Med 1999;42:762–771. [PubMed: 10502766]
19. Balu N, Chu B, Hatsukami TS, Yuan C, Yarnykh VL. Comparison between 2D and 3D high-resolution black-blood techniques for carotid artery wall imaging in clinically significant atherosclerosis. J Magn Reson Imaging 2008;27:918–924. [PubMed: 18383253]
20. Sirol M, Itskovich VV, Mani V, et al. Lipid-rich atherosclerotic plaques detected by gadofluorine-enhanced in vivo magnetic resonance imaging. Circulation 2004;109:2890–2896. [PubMed: 15184290]
21. Koktzoglou I, Li D. Submillimeter isotropic resolution carotid wall MRI with swallowing compensation: imaging results and semiautomated wall morphometry. J Magn Reson Imaging 2007;25:815–823. [PubMed: 17345637]
22. Wang J, Yarnykh VL, Hatsukami T, Chu B, Balu N, Yuan C. Improved suppression of plaque-mimicking artifacts in black-blood carotid atherosclerosis imaging using a multislice motion-sensitized driven-equilibrium (MSDE) turbo spin-echo (TSE) sequence. Magn Reson Med 2007;58:973–981. [PubMed: 17969103]
23. Scheffler K, Lehnhardt S. Principles and applications of balanced SSFP techniques. Eur Radiol 2003;13:2409–2418. [PubMed: 12928954]
24. Chung, YC.; Du, J.; Weale, P., et al. Carotid artery imaging at 3T: more signal from 3D imaging using a new 4-element coil. Proceedings of the 15th Annual Meeting of ISMRM; Berlin, Germany. 2997. abstract 683
25. Mani V, Itskovich VV, Aguiar SH, et al. Comparison of gated and non-gated fast multislice black-blood carotid imaging using rapid extended coverage and inflow/outflow saturation techniques. J Magn Reson Imaging 2005;22:628–633. [PubMed: 16215965]
26. Koktzoglou I, Chung YC, Mani V, et al. Multislice dark-blood carotid artery wall imaging: a 1.5 T and 3.0 T comparison. J Magn Reson Imaging 2006;23:699–705. [PubMed: 16555260]
27. Mugler, JP., 3rd; Wald, LL.; Brookeman, JR. T2-weighted 3D spin-echo train imaging of the brain at 3 Tesla: reduced power deposition using low flip-angle refocusing RF pulses. Proceedings of the 9th Annual Meeting of ISMRM; Glasgow, Scotland, UK. 2001. abstract 438
28. Busse RF, Hariharan H, Vu A, Brittain JH. Fast spin echo sequences with very long echo trains: design of variable refocusing flip angle schedules and generation of clinical T2 contrast. Magn Reson Med 2006;55:1030–1037. [PubMed: 16598719]
29. Alexander AL, Buswell HR, Sun Y, Chapman BE, Tsuruda JS, Parker DL. Intracranial black-blood MR angiography with high-resolution 3D fast spin echo. Magn Reson Med 1998;40:298–310. [PubMed: 9702712]
30. Jara H, Yu BC, Caruthers SD, Melhem ER, Yucel EK. Voxel sensitivity function description of flow-induced signal loss in MR imaging: implications for black-blood MR angiography with turbo spin-echo sequences. Magn Reson Med 1999;41:575–590. [PubMed: 10204883]
31. Koktzoglou I, Li D. Diffusion-prepared segmented steady-state free precession: Application to 3D black-blood cardiovascular magnetic resonance of the thoracic aorta and carotid artery walls. J Cardiovasc Magn Reson 2007;9:33–42. [PubMed: 17178678]
32. Isoda H, Kataoka M, Maetani Y, et al. MRCP imaging at 3.0 T vs. 1.5 T: preliminary experience in healthy volunteers. J Magn Reson Imaging 2007;25:1000–1006. [PubMed: 17410562]
33. Heverhagen JT. Noise measurement and estimation in MR imaging experiments. Radiology 2007;245:638–639. [PubMed: 18024445]
34. Rousson V, Gasser T, Seifert B. Assessing intrarater, interrater and test-retest reliability of continuous measurements. Stat Med 2002;21:3431–3446. [PubMed: 12407682]
35. Bland JM, Altman DG. Statistical methods for assessing agreement between two methods of clinical measurement. Lancet 1986;1:307–310. [PubMed: 2868172]
36. Park J, Mugler JP 3rd, Horger W, Kiefer B. Optimized T1-weighted contrast for single-slab 3D turbo spin-echo imaging with long echo trains: application to whole-brain imaging. Magn Reson Med 2007;58:982–992. [PubMed: 17969106]

37. Chung, YC.; Winner, M.; Park, J.; Raman, S.; Simonetti, OP.; Jerecic, R. T1-weighted 3D dark blood TSE for carotid artery disease imaging - preliminary experience. Proceedings of the 11th Annual Meeting of SCMR; Los Angeles, CA, USA. 2008. abstract 2137

38. Sarkar, R.; Moody, AR.; Leung, G. Effects of cardiac gating in high-resolution MRI of the carotid vessel wall. Proceedings of the 17th Annual Meeting of ISMRM; Honolulu, Hawai'i, USA. 2009. abstract 1825

39. Crowe LA, Keegan J, Gatehouse PD, et al. 3D volume-selective turbo spin echo for carotid artery wall imaging with navigator detection of swallowing. J Magn Reson Imaging 2005;22:583–588. [PubMed: 16161101]

40. Fan, Z.; Zuehlsdorff, S.; Lai, P.; Weale, P.; Chung, YC.; Li, D. 3D SPACE arterial wall imaging with prospective self-gating for motion compensation. Proceedings of the 17th Annual Meeting of ISMRM; Honolulu, Hawai'i, USA. 2009. abstract 1828

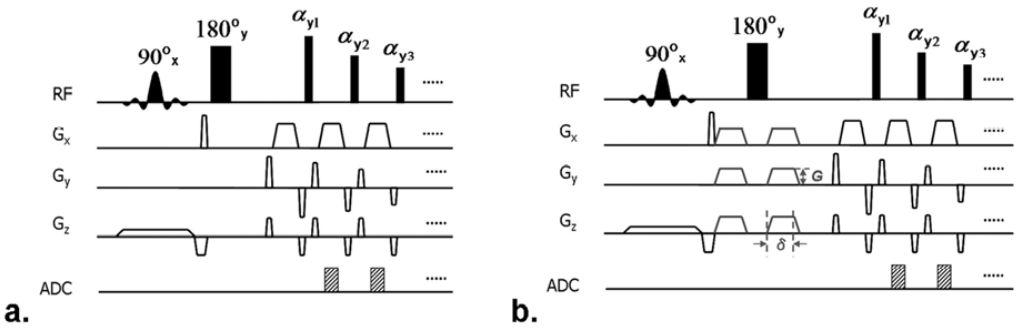

Figure 1.

Sequence diagram of the conventional SPACE sequence (a) and FSD-SPACE sequence (b). SPACE acquisition employs a slab-selective excitation RF pulse ($90°_x$) and a spatially nonselective refocusing ($180°_y$) pulse followed by a series of variable low-flip-angle nonselective refocusing pulses (α_{y1}, α_{y2}, α_{y3} …). The first readout is not recorded to exclude the initial high-level non-T2-weighted signal. In the FSD-SPACE sequence, two identical flow-sensitizing trapezoidal gradient pulses with a duration of δ = 3 ms and a magnitude of G = 12 mT/m are symmetrically placed before and after the first refocusing pulse in the readout, phase-encoding, and partition-encoding directions, respectively.

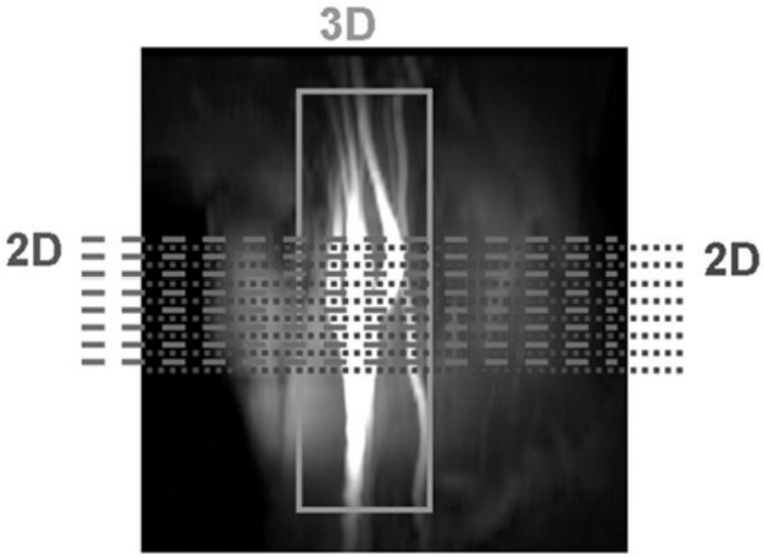

Figure 2.
Illustration of 2D TSE and 3D SPACE imaging coverages. Time-of-flight (TOF) sagittal maximum intensity projection (MIP) is used for imaging volume prescription. 2D TSE acquires contiguous 16 transverse slices through 2 scans (dashed and dotted lines). 3D SPACE acquires a coronal slab consisting of 80 slices (rectangle).

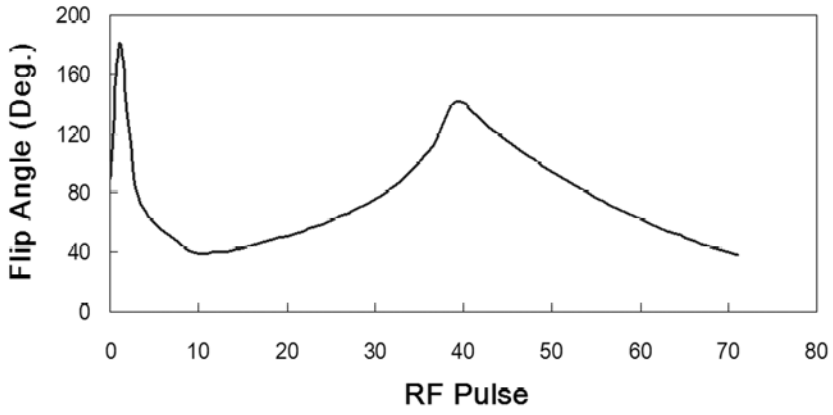

Figure 3.
Illustration of the variable-flip-angle scheme used in both SPACE and FSD-SPACE acquisitions in this work. A 90° slab-selective excitation RF pulse and a 180° nonselective refocusing RF pulse are followed by 70 variable-flip-angle nonselective refocusing RF pulses.

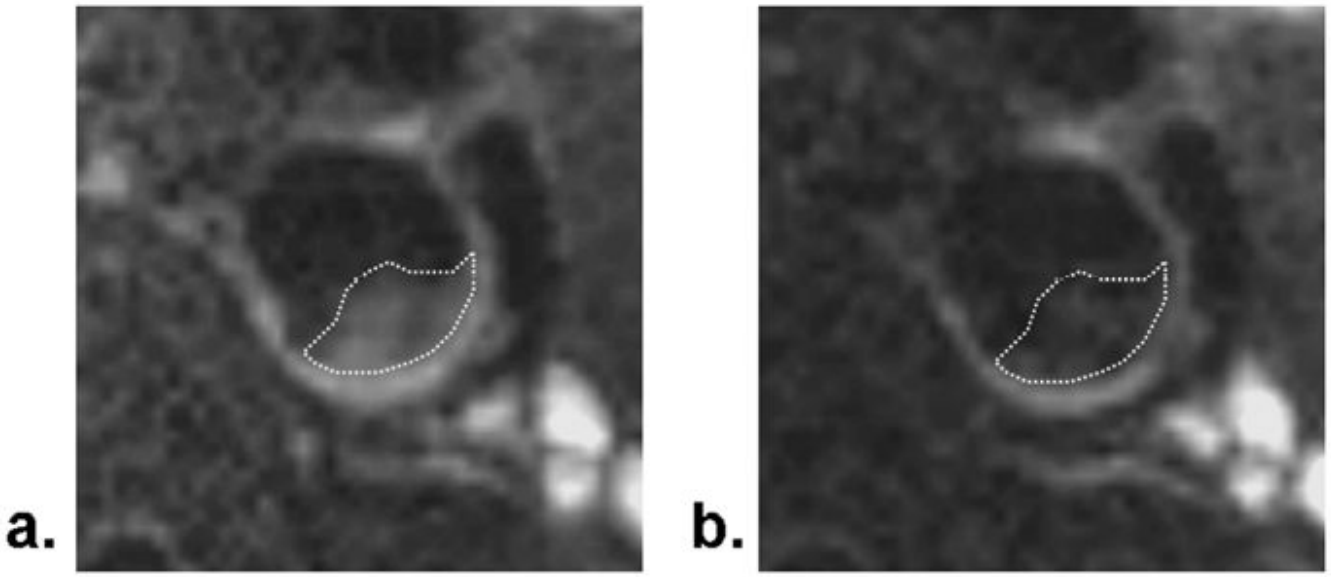

Figure 4.

Representative cross-sectional images, with and without the plaque-mimicking flow artifacts, reconstructed from SPACE (a) and FSD-SPACE (b) datasets, respectively. The artifactual region is first delineated on the SPACE image, shown as a closed dotted line, and the contour is then propagated to the FSD-SPACE image. Note that the contrast between this region and surrounding vessel wall is drastically boosted by the FSD preparation, minimizing the likelihood of mistaking the artifacts for a plaque. However, overall signal attenuation is appreciable on the FSD-SPACE image.

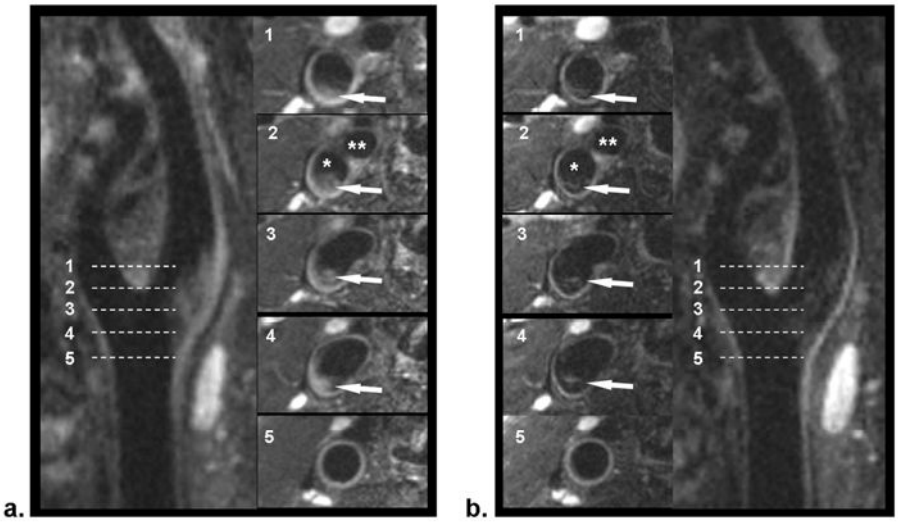

Figure 5.

Comparison of location-matched SPACE (a) and FSD-SPACE (b) images acquired from a healthy volunteer. Using multiplanar reconstruction (MPR), both longitudinal and cross-sectional views of the carotid artery can be visualized. The FSD preparation can dramatically suppress the residual blood signal (arrows) shown on SPACE images, thus resulting in larger apparent lumen and higher wall-lumen contrast. The locations of the five cross-sectional images (No. 1-5) are indicated by the dashed line on the longitudinal images. *, internal carotid lumen; **, external carotid lumen.

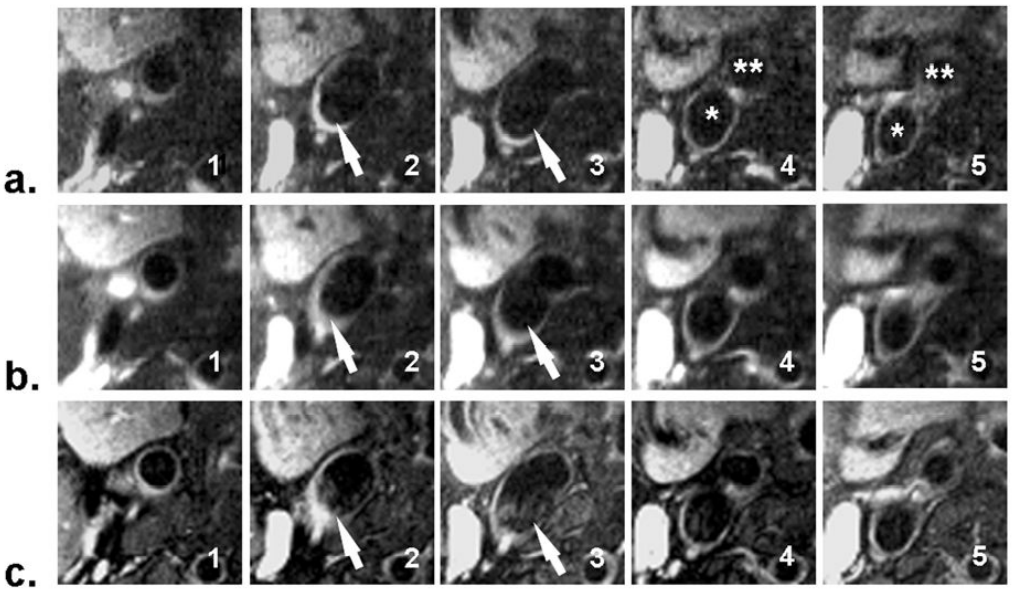

Figure 6.

Comparison of location-matched cross-sectional FSD-SPACE (a and b) and 2D SB-TSE (c) images of the carotid bifurcation from a healthy volunteer. Shown are 0.63-mm-thick FSD-SPACE images (a), 3-mm-thick FSD-SPACE images (b), and 3-mm-thick 2D TSE images (c). Images 1-5 (foot-to-head) from both techniques show similar 2-weighted contrast. Compared with the 2D technique, the FSD-SPACE sequence offers better blood signal suppression (arrows). The isotropic high-spatial-resolution images (a) provide sharper arterial wall delineation but lower wall signal than other groups (b and c). *, internal carotid lumen; **, external carotid lumen.

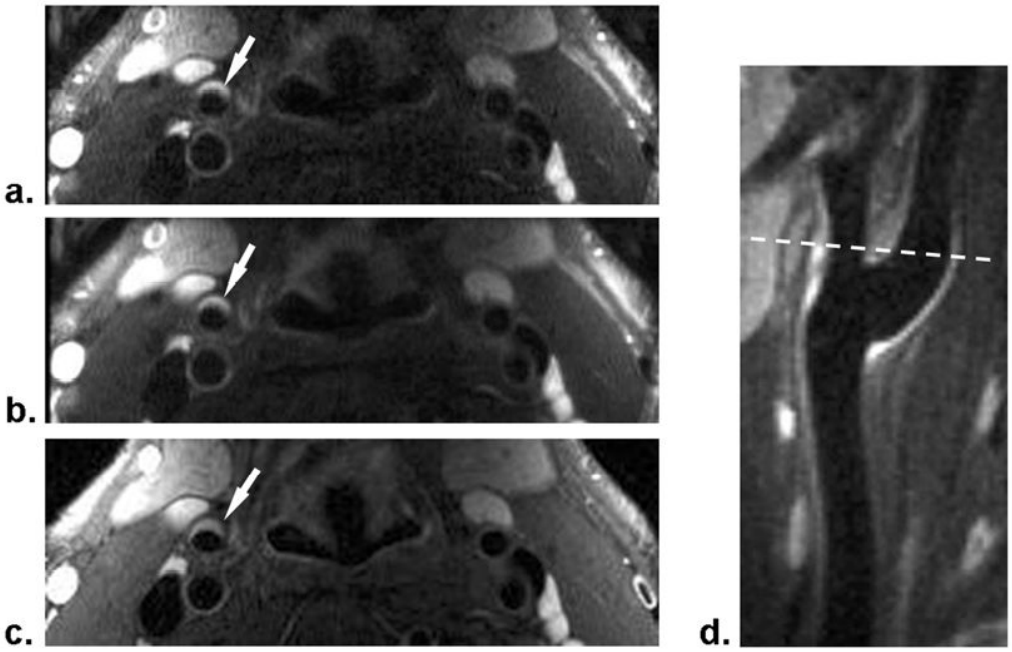

Figure 7.
Images illustrating the capability of flexible visualization of the carotids using 3D MRI and multi-planar reconstruction (MPR) technique. Vessel thickening at the bifurcation in a healthy volunteer is clearly depicted on the 0.63-mm-thick (a) and 3-mm-thick (b) transverse FSD-SPACE images and the 3-mm-thick SB-TSE image (c). With MPR, however, 3D FSD-SPACE is capable of offering valuable information on the degree and extent of the thickening, particularly through a longitudinal view (d).

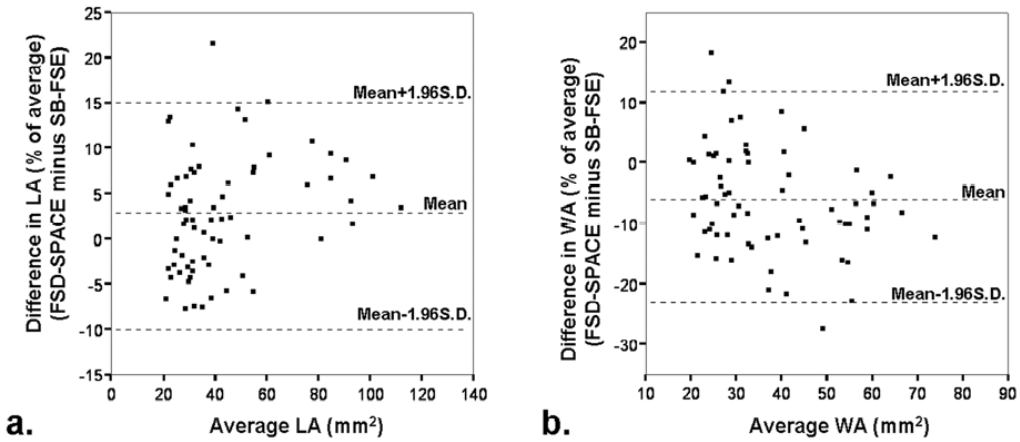

Figure 8.

Bland-Altman plots of the percentage difference versus the mean for two morphological measurements: carotid arterial lumen area (a) and carotid arterial wall area (b). Measurements at a total of 70 transverse locations obtained from FSD-SPACE and SF-TSE are shown to be in a good agreement. However, FSD-SPACE images show an averagely 2.7±6.3% larger lumen area and an averagely 5.6±8.8% smaller vessel wall area. LA: lumen area; WA: wall area.

Table 1

Signal and Morphological Measurement Comparisons between SPACE and FSD-SPACE Sequences

	$aSNR_l$	**$aSNR_w$**	**$aCNR_{w-l}$**	**$aCNR_{w-rb}$**	**aLA**
SPACE	6.5 ± 2.4	14.2 ± 3.6	7.7 ± 1.8	0.8 ± 2.3	61.4 ± 23.5
FSD-SPACE	3.6 ± 1.1	10.7 ± 2.2	7.1 ± 1.4	4.7 ± 2.2	77.9 ± 30.6
p-value	< 0.001	< 0.001	0.025	< 0.001	< 0.001

Note: Data are presented as mean ± standard deviation. $aSNR_l$: apparent carotid lumen SNR; $aSNR_w$: apparent carotid wall SNR; $aCNR_{w-l}$: apparent carotid wall-lumen CNR; $aCNR_{w-rb}$: apparent CNR between the intraluminal residual blood region and carotid wall; aLA: apparent carotid lumen area.

Table 2

Signal and Morphological Measurement Comparisons between SB-TSE and FSD-SPACE Sequences

	$aCNR_{w-l}$	$aCNR_{uv}$	LA	WA
SB-TSE	6.8 ± 2.1	7.4 ± 2.3	42.5 ± 21.3	38.7 ± 14.8
FSD-SPACE	7.0 ± 2.1	28.0 ± 8.2	44.1 ± 23.1	36.0 ± 12.9
p-value	0.329	< 0.001	< 0.001	< 0.001

Note: Data are presented as mean ± standard deviation. $aCNR_{w-l}$: apparent carotid wall-lumen CNR; $aCNR_{uv}$: apparent carotid wall-lumen CNR adjusted by voxel volume; LA: carotid lumen area; WA: carotid wall area.